Journal of Catalysis 231 (2005) 172-180

Microkinetic modelling of the dehydrogenation of ethylbenzene to styrene over unpromoted iron oxides

Achim Schüle[a], Osama Shekhah[b], Wolfgang Ranke[b], Robert Schlögl[b], Grigorios Kolios[a,*]

[a] Institute of Chemical Processes Engineering, University of Stuttgart, Böblinger Str. 72, D-70199 Stuttgart, Germany
[b] Department Inorganic Chemistry, Fritz-Haber-Institute of the MPG, Faradayweg 4-6, D-14195 Berlin, Germany

* Corresponding author: e-mail kolios@icvt.uni-stuttgart.de, phone +49/711–6412214, fax +49/711–6412242

Submitted 28 June 2004; accepted 12 January 2005

Abstract
A vast amount of surface science experiments provides a detailed qualitative picture of the mechanisms governing the catalytic dehydrogenation of ethylbenzene (EB) to Styrene (St) over unpromoted iron oxide. Also values of kinetic and energetic parameters for adsorption and desorption are available. We present a methodology of kinetic modelling based upon this knowledge, aiming at an accurate prediction of the behaviour of the technical catalysts including deactivation and regeneration. This paper contains the detailed kinetic model and the procedure followed for determining the kinetic parameters.

Keywords: Microkinetic model, dehydrogenation, ethylbenzene, styrene, iron oxide, deactivation, coking, solid phase transformation

1. Introduction

The power of microkinetic modelling [1] of a catalytic process based on data obtained from surface science studies was already demonstrated for ammonia synthesis [2-4] as reviewed in [5]. The catalyst in this system can be considered invariant. However, including gas-solid-interactions in catalytic reaction processes usually results in a change of state of the catalyst. In most cases these solid state transformations are connected with catalyst deactivation.

A typical example is the potassium promoted iron oxide catalyst used for styrene synthesis through dehydrogenation of ethylbenzene. It is known that the styrene catalyst undergoes significant changes during its lifetime. This involves physical degradation, formation of carbonaceous deposits and an inherent phase change of Fe_2O_3 (hematite) under reaction conditions towards Fe_3O_4 (magnetite), which exhibits only a minor catalytic activity [6,7]. Nevertheless, kinetic expressions published by several groups [8-10] neglect these transient effects occurring under normal operating conditions. Therefore, such standard kinetic models have clear practical restrictions. They are not suitable to describe the catalytic behaviour except at a certain stationary state. Model based process optimization and assessment of the potential of novel reactor concepts become infeasible that way [8,11,12]. The shortcomings of available kinetic models definitely affect the progress in engineering of the styrene process. Clearly, it is infeasible to resolve the mechanism of the process studying the behaviour of the real catalyst under practically relevant conditions. The aim to analyse individual aspects isolated under well defined conditions led to a surface science approach. This approach relies on detailed conversion measurements and analyses of gas-surface interactions for monocrystalline model surfaces [13-20]. Details of the experimental set-up and of the kinetic measurements are presented in [19-21]. The most comprehensive set of experimental data so far is available for epitactically grown single crystal films (SCF) of iron oxide representing a generic model of the real catalyst. These experiments provide:

- intrinsic reaction rates without falsification by diffusional limitations;
- time resolved information of the changes of the film composition in the reaction atmosphere;

- kinetic and equilibrium parameters for the adsorption of individual components of the reaction mixture on the model surface.

The available information allows for the postulation of a qualitative mechanistic model of ethylbenzene dehydrogenation over iron oxides.

However, the final goal is to translate this information to technical conditions. A model-based approach is employed in order to bridge the gap between the observations made on ideal surfaces and the behaviour of real catalysts. The chosen approach is based on the standard modelling procedure applied in chemical reaction engineering: the task is mainly to compute a set of parameters of the kinetic reactor model such that simulation results resemble the measured values as close as possible. The novelty of the present contribution consists in the structure of the model and in the experimental basis used for adjusting the free model parameters.

The underlying mechanistic catalyst model is introduced in section 2 and the model equations in section 3. Finally, parameterisation and validation of the model is discussed in section 4.

2. Catalyst model

The primary goal of our approach is the mechanistic description of the relevant physico-chemical gas-solid-interactions during dehydrogenation of ethylbenzene to styrene over iron oxide, thus the derivation of a mechanistic catalyst model. The model is represented by a set of stoichiometric equations describing the main reaction, the redox processes and coke formation on the catalyst surface. Side reactions towards benzene and toluene are neglected. Overall activity of the surface includes the contribution of clean iron oxide and coked areas. The model is based on the following assumptions: overall conversion is split up into individual steps of adsorption, surface reaction and desorption; gas-solid reactions related with formation and gasification of coke and phase transformation of iron oxide are considered as single-step reactions.

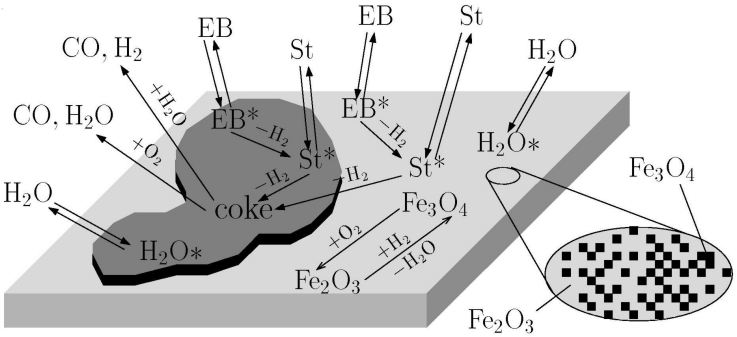

Figure 1:
Schematic representation of the mechanistic model of ethylbenzene dehydrogenation over iron oxide.

Figure 1 shows the considered reaction steps. The surface is assumed to be inhomogeneous, consiting of areas of clean iron oxide and those covered by coke. The iron oxide layer is considered as a mixture of hematite and magnetite depending on the oxygen content. The feed components water and ethylbenzene as well as styrene adsorb at the surface. Thermal desorption mass spectroscopy (TDS) confirms the existence of the respective surface species [17]. The adsorption-desorption equilibrium is described by the following stoichiometric equations (adsorption: equations (1) to (3), desorption: equations (4) to (6)):

$$EB + * \rightarrow EB* \quad (1)$$
$$St + * \rightarrow St* \quad (2)$$
$$H_2O + * \rightarrow H_2O* \quad (3)$$

} *each on iron oxide and coke*

$$EB* \rightarrow EB + * \quad (4)$$
$$St* \rightarrow St + * \quad (5)$$
$$H_2O* \rightarrow H_2O + * \quad (6)$$

} *each on iron oxide and coke*

Only vague information exists on the conversion of adsorbed ethylbenzene to styrene. Dehydrogenation of EB via H-abstraction by basic surface oxygen located at defect sites has been proposed [16] which would leave two OH groups at the surface. Direct recombinative desorption of H_2 is intuitively not the most likely path for hydrogen removal. An alternative would be desorption in form of H_2O under consumption of surface oxygen. Reoxidation could be possible by dissociative adsorption of water or oxygen added to the feed (Mars-Van Krevelen mechanism). However, it has been shown that this stoichiometric reaction would result in a much faster substrate reduction than actually observed [7]. Since the actual mechanism is unknown so far, the dehydrogenation of ethylbenzene to styrene is formally regarded as a single-step surface reaction (equation (7)). The hydrogen formed is assumed to be directly released to the gas atmosphere.

$$EB* \rightarrow St* + H_2 \quad (7) \quad \textit{on iron oxide and coke}$$

Styrene is indicated as the precursor of coke formation [22,23] (equation(8)). According to [22], the carbonaceous deposits are of poly-aromatic nature with H/C ratio of 0,5:

$$St^* \rightarrow coke + 2\,H_2 \qquad (8) \qquad \text{on iron oxide and coke}$$

Own analyses using Auger electron spectroscopy suggest a graphitic structure of the carbonaceous surface layer.
The redox reactions of the iron oxides are formally described by equations (9) and (10). Hydrogen oxidation or water dissociation as the reverse reaction is taken into account implicitly through their linear dependency on equations (9) and (10). This is justified due to the high rates of these reaction steps.

$$3Fe_2O_3 + H_2 \rightarrow 2Fe_3O_4 + H_2O \qquad (9)$$

$$4Fe_3O_4 + O_2 \rightarrow 6Fe_2O_3 \qquad (10)$$

Removal of coke by gasification in water vapour or oxygen containing atmosphere (equations (11) and (12)) completes the reaction scheme.

$$coke + 8H_2O \rightarrow 8CO + 10H_2 \qquad (11)$$

$$coke + 5O_2 \rightarrow 8CO + 2H_2O \qquad (12)$$

3. Model equations

The kinetic reactor used for conversion measurements over monocrystalline model surfaces is described in [21]. Its design is intended to establish a stagnation point flow pattern in the chamber above the catalyst sample. A simple continuous stirred tank reactor (CSTR) model is employed for describing the set-up in the present context (Figure 2). This is justified by the low conversions obtained during the kinetic measurements (max. 10%) producing only slight changes in the composition of the reaction mixture. This assumption is also consistent with the observed uniform surface composition during conversion experiments. Further, constant temperature and pressure are assumed. Hence, the model consists of dynamic mass balances of the gaseous, adsorbed and solid phase components. Two parallel reaction paths with different rates are considered for the reactions (1) to (8) over coke and iron oxide as discussed in the previous section.

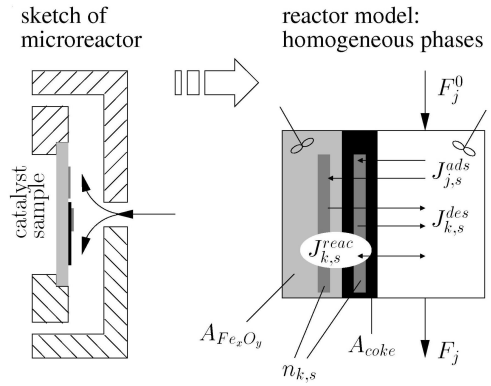

Figure 2:
Reactor model underlying the kinetic modelling. Left: sketch of the micro reactor developed for kinetic measurements [19]. Right: reactor model indicating the phases considered.

The total surface areas covered by coke and iron oxide are given through:

$$A_{coke} = N_{coke} \cdot a_{coke} \quad , \quad a_{coke} = const.$$

$$A_{Fe_xO_y} = A_0 - A_{coke} \quad , \quad A_0 = const.$$

Therein, a_{coke} specifies the molar surface density of the coke layer. Its thickness on the deactivated catalyst was estimated to about 10 Å using Auger electron spectroscopy. Assuming the atomic density of graphite, this corresponds to about three monolayers. A_0 is the total surface area given by the geometry of the catalyst sample.

The iron oxide surface is assumed as a pseudo-homogeneous solid since oxygen is known to have a high mobility in the lattice at reaction temperature [24]. Conversion of hematite to magnetite is described through a uniform continuous depletion of oxygen and vice versa. Accordingly, the iron oxide surface model is represented through a pseudo-component varying continuously between magnetite and hematite. The fraction of each oxide is back calculated from the oxygen to iron ratio of the pseudo homogeneous phase. Molar balances of the lattice elements yield the hematite fraction to:

$$x_{Fe_2O_3} = \frac{3 \cdot N_O - 4 \cdot N_{Fe}}{N_O - N_{Fe}} \quad , \quad N_{Fe} = const. \qquad (13)$$

N_{Fe} is the constant number of moles of iron in the catalyst sample and N_0 is the number of moles of lattice oxygen, which is variable. The activity of the iron oxide is variable depending on the hematite and magnetite content.
The balance equations are expressed in moles. The unknowns of the system N, the number of moles of each component, are coupled through mass exchange terms J.
Balances of gaseous components:

$$\frac{dN_j}{dt} = F_j^0 - F_j - \sum_s J_{j,s}^{ads} + \sum_s J_{j,s}^{des} + \sum_i \nu_{i,j} \cdot J_i^{reac} \quad , \quad i \in \{(j,s),(k,s),p\}$$

Balances of adsorbed species:

$$\frac{dN_{k,s}}{dt} = J_{k,s}^{ads} - J_{k,s}^{des} + \sum_i \nu_{i,k} \cdot J_i^{reac} \quad , \quad i \in \{(k,s)\}$$

Solid phase balances:

$$\frac{dN_s}{dt} = \sum_i \nu_{i,s} \cdot J_i^{reac} \quad , \quad i \in \{(j,s),(k,s),p\}$$

$$j \in \{He, H_2O, EB, St, H_2, O_2, CO\}$$

$$k \in \{EB^*, St^*, H_2O^*\}$$

$$s \in \{Fe_xO_y, coke\} \quad , \quad p \in \{Fe_2O_3, Fe_3O_4\}$$

The balance of the solid pseudo-component iron oxide is expressed in terms of number of moles of lattice oxygen.

The constant pressure condition of the gas phase yields an expression of the outlet molar flow in terms of the feed stream and the mass exchange streams:

$$\frac{dN^{gas}}{dt} = 0 \quad \Rightarrow \quad F = F^0 - \sum_k \sum_s J_{k,s}^{ads} + \sum_k \sum_s J_{k,s}^{des} + \sum_i \sum_j \nu_{i,j} \cdot J_i^{reac}$$

All exchange and conversion streams must be expressed as functions of the unknowns in order to obtain a well-defined system.

Adsorption and desorption streams are defined for EB, St and H_2O according to stoichiometric equations (1) to (6). For all other components they are explicitly set to zero.

Adsorption is assumed to be non-activated and non-dissociative with sticking coefficients $\sigma_{j,s}$ equal to unity:

$$J_{j,s}^{ads} = \frac{p_j}{\left(2\pi \cdot R \cdot T \cdot M_j\right)^{1/2}} \cdot \sigma_{j,s} \cdot \left(1 - \Theta_s\right) \cdot A_s \quad , \quad \begin{matrix} j \in \{EB, St, H_2O\} \\ s \in \{Fe_2O_3, Fe_3O_4, coke\} \end{matrix}$$

$$\Theta_s = \frac{\sum_k n_{k,s}}{n_s^{sat.}} \quad , \quad n_{k,s} = \frac{N_{k,s}}{A_s} \quad , \quad n_s^{sat.} = const. \quad , \quad k \in \{EB^*, St^*, H_2O^*\}$$

Therein, $n_s^{sat.}$ describes the maximum surface concentration of components on the surfaces. In [17] the respective value for EB, St and H_2O on magnetite surface was derived theoretically and compared to experimental findings. We assume equal maximum surface concentrations for all components on magnetite as well as on hematite.

Desorption kinetics are derived from thermal desorption mass spectroscopy (TDS) and can be described by the following expression:

$$J_{k,s}^{des} = f_{k,s} \cdot e^{\left\{\frac{-E_{k,s}^{des}}{RT}\right\}} \cdot n_{k,s} \cdot A_s \quad , \quad \begin{matrix} k \in \{EB^*, St^*, H_2O^*\} \\ s \in \{Fe_2O_3, Fe_3O_4, coke\} \end{matrix}$$

The reaction steps postulated in equations (7) to (12) are considered as single-step reactions. Accordingly, the reaction streams are written as follows:

- gasification reactions involving gas phase components:

$$J_{j,s}^{reac} = k_{j,s}^0 \cdot e^{\left\{\frac{-E_{j,s}^{reac}}{R}\left(\frac{1}{T} - \frac{1}{T_0}\right)\right\}} \cdot A_s \cdot p_j \quad , \quad \begin{matrix} j \in \{H_2O, O_2\} \\ s \in \{coke\} \end{matrix}$$

- surface reactions involving adsorbed species:

$$J_{k,s}^{reac} = k_{k,s}^0 \cdot e^{\left\{\frac{-E_{k,s}^{reac}}{R}\left(\frac{1}{T} - \frac{1}{T_0}\right)\right\}} \cdot n_{k,s} \cdot A_s \quad , \quad \begin{matrix} k \in \{EB^*, St^*\} \\ s \in \{Fe_2O_3, Fe_3O_4, coke\} \end{matrix}$$

Finally, the fluxes related to the phase transformation of either iron oxide to the other by reduction and oxidation are derived based on the principle of non-equilibrium thermodynamics [25]. According to this principle, equilibrium composition of the Fe-O system in the solid phase is determined by the composition of the gas atmosphere. The kinetics follow linear driving force relations, where the chemical affinity of the reaction, X, is considered as the driving force [25]:

$$J_p^{reac} = \left(-\sum_q L_{p,q} \cdot \frac{\mathrm{X}_q}{T} \right) \cdot x_p \quad , \quad \begin{matrix} p \in \{Fe_2O_3, Fe_3O_4\} \\ q \in \{H_2, O_2\} \end{matrix}$$

$$\mathrm{X}_q = \sum_l \nu_{l,q} \cdot \mu_l \qquad l \in \{Fe_2O_3, Fe_3O_4, H_2O, H_2, O_2\}$$

$$\mu_l = \mu_l^0(p_0,T) + RT \cdot \ln(a_l) \quad , \quad \begin{cases} a_l = 1 & , \ l = Fe_2O_3, Fe_3O_4 \\ a_l = p_l / p_0 & , \ l = H_2O, H_2, O_2 \end{cases}$$

Finally, the individual interactions on hematite and magnetite need to be replaced by a single mass exchange term for the balance equations. A lever arm rule applies for the overall interactions of the gase phase with the iron oxide surface:

$$J_{m,Fe_xO_y}^{ads/des/reac} = J_{m,Fe_2O_3}^{ads/des/reac} \cdot x_{Fe_2O_3} + J_{m,Fe_3O_4}^{ads/des/reac} \cdot \left(1 - x_{Fe_2O_3}\right), \ m = \{EB, St, H_2O, EB^*, St^*, H_2O^*\}$$

4. Parameter determination and discussion

The overall set of physico-chemical interactions of the catalyst model shown in Figure 1 includes in total 31 parameters as introduced in the previous section. Part of them (twelve parameters), i.e. the frequency factors and energies for desorption of EB, St and H_2O from hematite and magnetite are directly measurable [16-18].

The desorption energy of ethylbenzene over carbonaceous species is directly determined from recent measurements [26]. The respective parameter values for styrene are derived based on the assumption of identical frequency factors and slightly higher activation energy than for ethylbenzene similar to the findings on different iron oxide surfaces [17]. The parameters of water desorption from coke are determined analogously. The set of desorption parameters is summarised in Table 2.

The parameter values determined for pure components also hold for the reactive system under the assumption of insignificant multi-component interactions of adsorbed species. This is justified by the low surface coverage under the conditions of the conversion experiments [14].

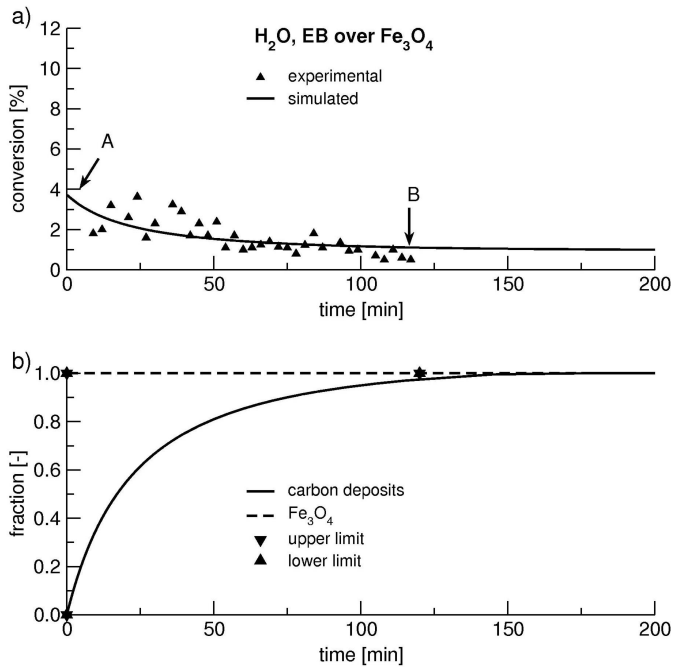

Figure 3:
Experimental basis of subsystem 1 for adjusting the parameters of the kinetic model (symbols) and simulation results (lines). a) Evolution of conversion with time of pure dehydrogenation over a surface initially consisting of magnetite. b) Surface composition and coverage by carbon deposits over time.
Conditions: T=870K, p_{tot}=1bar, p_{H2O}=3400Pa, p_{EB}=340Pa, He carrier gas, V= 25*10^{-6}Nm^3/min.

The remaining 13 parameters have been adjusted to conversion experiments in the kinetic reactor [19-21]. Three test series have been considered for parameter fitting:

1. nonoxidative dehydrogenation over initially clean magnetite surface (Figure 3);
2. nonoxidative dehydrogenation over initially clean hematite surface (Figure 4);
3. oxidative dehydrogenation over initially clean hematite surface (Figure 6).

The conversion measurements have been performed mainly at a temperature of 870K and a total pressure of 1bar [7,19]. Experimental data at varying temperatures have been acquired so far for the subsystem 2 (Figure 5). The available experimental data are gas phase concentrations measured by gas chromatography (GC) and data from off-line surface analyses. The surface analysis data are labelled in the conversion diagrams. Table 1 summarises the iron oxide fractions derived from Auger electron spectroscopy (AES) and low-energy electron diffraction (LEED). The surface fraction covered by coke is determined by AES and temperature programmed oxidation (TPO) [19]. These experimental data form the basis for fitting the unknown parameters of the kinetic model stated above.

We apply a stepwise parameter fitting procedure, which addresses the different subsystems. The advantage of this strategy is that only a reduced number of interactions are active at once and artificial cross correlations between parameters can be avoided.

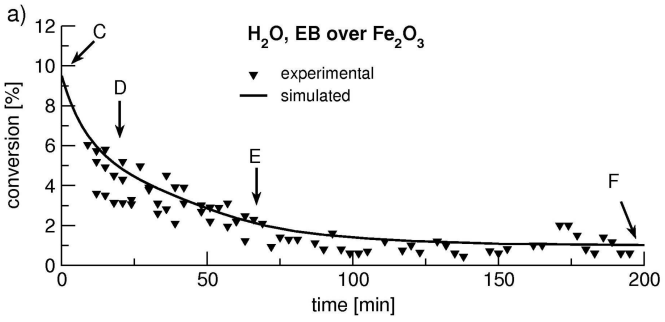

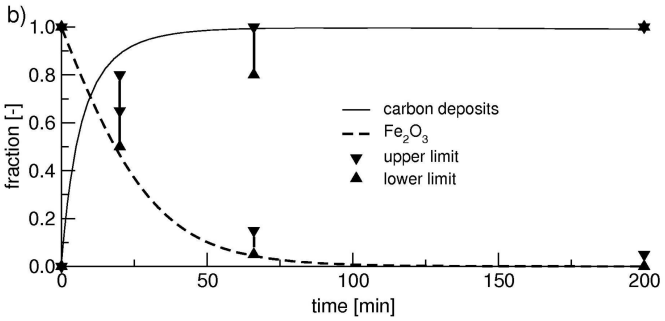

Figure 4:
Experimental basis of subsystem 2 for adjusting the parameters of the kinetic model (symbols) and simulation results (lines). a) Evolution of conversion with time of pure dehydrogenation over a surface initially consisting of hematite. b) Surface composition and coverage by carbon deposits over time.
Conditions: T=870K, p_{tot}=*1*bar, p_{H2O}=3400*Pa*, p_{EB}=340*Pa*, He carrier gas, V= 25*10^{-6}*Nm^3/min.*

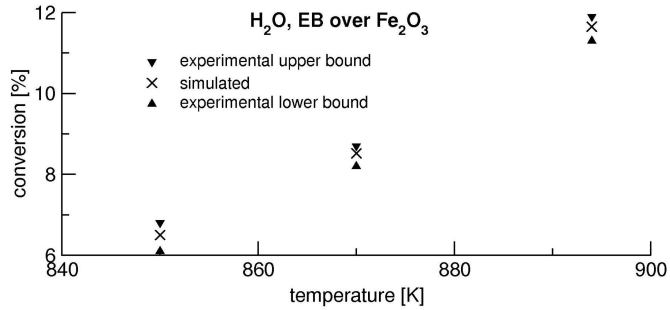

Figure 5:
Experimental basis of subsystem 2 for adjusting the parameters of the kinetic model (symbols) and simulation results (lines). Temperature dependent initial conversion of pure dehydrogenation on a clean hematite surface.
Conditions: p_{tot}=*1*bar, p_{H2O}=3400*Pa*, p_{EB}=340*Pa*, He carrier gas, V= 25*10^{-6}*Nm^3/min.*

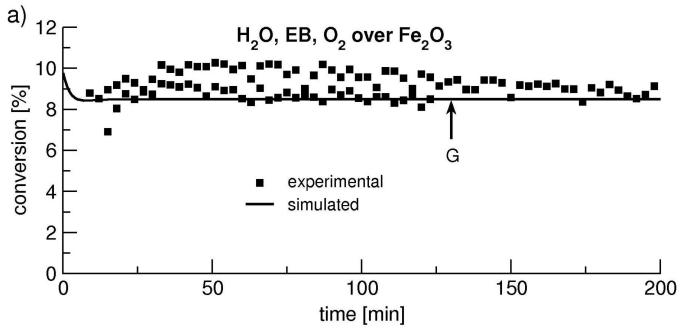

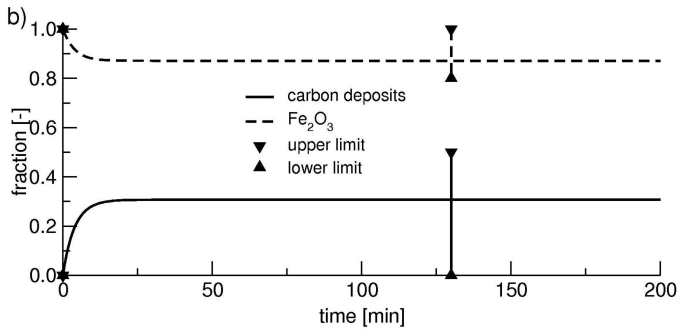

Figure 6:
Experimental basis of the complete system for adjusting the parameters of the kinetic model (symbols) and simulation results (lines). a) Evolution of conversion with time of dehydrogenation in presence of oxygen over a surface initially consisting of hematite. b) Surface composition and coverage by carbon deposits over time.
Conditions: T=870K, p_{tot}=*1*bar, p_{H2O}=3400*Pa*, p_{EB}=340*Pa*, He carrier gas, V= 25*10^{-6}*Nm^3/min.*

Table 1:
Iron oxide composition and degree of surface coverage by carbonaceous deposits (both from surface analysis) and measured conversion over epitactically grown, mono-crystalline surfaces at : T=870K, p_{tot}=*1*bar, p_{H2O}=3400*Pa*, p_{EB}=340*Pa*, He carrier gas, V= 25*10^{-6}*Nm^3/min*.

identifier	iron oxide composition		coke deposition	conversion
	$x_{Fe_2O_3}[-]$	$x_{Fe_3O_4}[-]$	$\Theta_{coke}[-]$	$X_{EB}[\%]$
A	0.0	1.0	0.0	3.5
B	0.0	1.0	1.0	0.95
C	1.0	0.0	0.0	9.0
D	0.50-0.65	0.35-0.50	0.5-0.8	–
E	0.05-0.15	0.85-0.95	> 0.8	–
F	< 0.05	> 0.95	1.0	0.95
G	> 0.80	< 0.20	< 0.5	–

Table 2:
Stoichiometric equations considered and parameters for corresponding rate equation.

desorption	surface	$f_{k,s}[\frac{1}{s}]$	$E^{des}_{k,s}[\frac{J}{mol}]$	reference
EB* → EB + *	Fe_2O_3	$1 \cdot 10^{12}$	$64 \cdot 10^3$	[16]
	Fe_3O_4	$1 \cdot 10^{12}$	$86 \cdot 10^3$	[16]
	coke	$5 \cdot 10^{14}$	$65 \cdot 10^3$	[25]
St* → St + *	Fe_2O_3	$5 \cdot 10^{12}$	$73 \cdot 10^3$	[16]
	Fe_3O_4	$3 \cdot 10^{11}$	$118 \cdot 10^3$	[16]
	coke	$5 \cdot 10^{14}$	$70 \cdot 10^3$	[25]
H_2O* → H_2O + *	Fe_2O_3	$1 \cdot 10^{13}$	$63 \cdot 10^3$	[18]
	Fe_3O_4	$2.4 \cdot 10^{-6}$ [a]	$65 \cdot 10^3$	[17]
	coke	$1 \cdot 10^{12}$	$50 \cdot 10^3$	[25]
surface reaction	surface	$k^0_{j,s}[\frac{1}{s}]$	$E^{reac}_{j,s}[\frac{J}{mol}]$	reference
EB* → St* + H_2	Fe_2O_3	$2.1 \cdot 10^2$	$1.6 \cdot 10^5$	this work
	Fe_3O_4	$k(870K) = 9.07 \cdot 10^3 \frac{1}{s}$		this work
	coke	$k(870K) = 1.53 \cdot 10^5 \frac{1}{s}$		this work
St* → coke* + 2 H_2	Fe_2O_3	$k(870K) = 1.08 \cdot 10^1 \frac{1}{s}$		this work
	Fe_3O_4	$k(870K) = 1.42 \cdot 10^{-1} \frac{1}{s}$		this work
	coke	$k(870K) = 1.70 \cdot 10^1 \frac{1}{s}$		this work
gas-solid-reaction		$k(T)[\frac{mol}{s \cdot cm^2}]$		reference
coke* + 8 H_2O → 8 CO + 10 H_2		$k(870K) = 1.42 \cdot 10^{-13}$		this work
coke* + 5 O_2 → 8 CO + 2 H_2O		$k(870K) = 1.76 \cdot 10^{-9}$		this work
phase transformation		$L_{p,1}[\frac{mol^2 K}{J \cdot s}]$	$L_{p,2}[\frac{mol^2 K}{J \cdot s}]$	reference
3 Fe_2O_3 + H_2 → 2 Fe_3O_4 + H_2O		$1.5 \cdot 10^{-13}$	$1.0 \cdot 10^{-17}$	this work
4 Fe_3O_4 + O_2 → 6 Fe_2O_3		$1.0 \cdot 10^{-17}$	$1.3 \cdot 10^{-13}$	this work

[a]) [cm^2/s] due to second order relation $J^{des}_{k,s} = J^{des}_{k,s}((n_{k,s})^2)$

Starting point of the parameter fitting is the behaviour of a water-ethylbenzene feed over magnetite model catalysts (Figure 3). All interactions related to the hematite surface are inactive. Furthermore, no phase change takes place, as no oxygen is present. The change in conversion over time is attributed to coke formation. Surface analysis by AES and TPO clearly indicates complete coverage of the surface with coke (labels B and F) [19]. The evolution of conversion with time and the

build-up of carbon deposits allows for determination of the values of k_{EB*,Fe_3O_4}, k_{St*,Fe_3O_4}, $k_{EB*,coke}$, $k_{St*,coke}$ and $k_{H_2O,coke}$. Figure 3 indicates the decrease in conversion directly related to the increasing surface coverage by coke. The steady state conditions at the end of the experiment correlate to the activity of the carbon deposits only.

Next, a water-ethylbenzene feed over hematite is considered (Figure 4). Processing this data set provides the values of the parameters k_{St*,Fe_2O_3}, $k_{Fe_2O_3,H_2}$ and $k_{Fe_3O_4,H_2}$. Moreover, conversion measurements over hematite at different temperatures are available for the determination of activation energy E^{reac}_{EB*,Fe_2O_3} and pre-exponential factor k_{EB*,Fe_2O_3} on hematite. Figure 5 depicts the measured conversion at three different temperatures along with the simulated values.
Finally, the addition of oxygen to the process is considered (Figure 6). Starting from hematite, all interactions become active and allow for the determination of the remaining parameters, i.e. $k_{O_2,coke}$, $k_{Fe_2O_3,O_2}$ and $k_{Fe_3O_4,O_2}$. The complete set of the model parameters is summarised in Table 2.

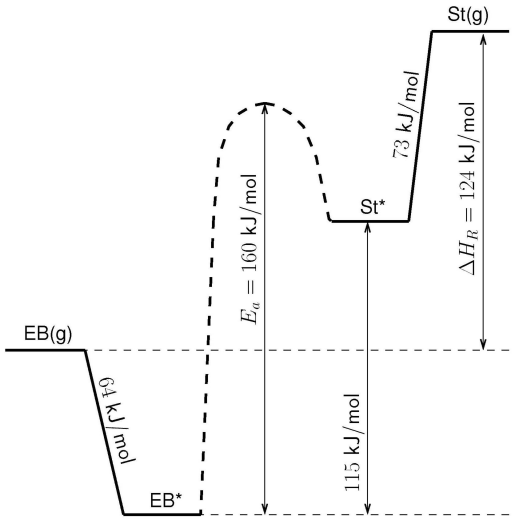

Figure 7:
Energy diagram of activation energies for the overall transformation from ethylbenzene to styrene on hematite.

Figure 7 presents the energy diagram displaying activation energies of the steps occurring during transformation from ethylbenzene to styrene. The adsorption energies of ethylbenzene and styrene are experimentally verified. The estimated value of the apparent activation energy of the conversion of adsorbed ethylbenzene to styrene (equation (7)) is thermodynamically consistent.

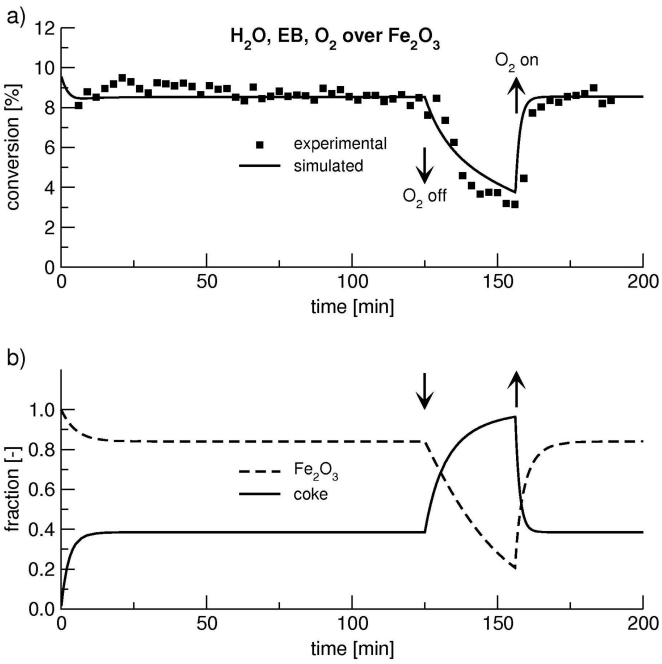

Figure 8:
Validation experiment for the kinetic model (symbols) and simulation results (lines). ↓: switching off oxygen in the feed; ↑: switching on oxygen in the feed.
Conditions: T=870K, p_{tot}=1bar, p_{H2O}=3400Pa, p_{EB}=340Pa, He carrier gas, V= 25*10^{-6}Nm^3/min.

The kinetic model is validated applying the dynamic response of the system to a step-change of the feed composition. The experiment starts with a fresh hematite model catalyst and a feed stream of water, ethylbenzene and oxygen. After 120min the oxygen supply is interrupted for 30min. Figure 8 shows an excellent agreement between the measured and simulated conversion.

We conclude that the catalyst model and the used parameter set adequately describe the behaviour of the styrene synthesis process over ideal, monocrystalline surfaces which are free from mass transport limitations. The model also describes the observed catalyst deactivation taking into account transformations of the catalyst phase and formation of carbonaceous deposits. The validity of the set of parameters is confirmed by the fact that parameters derived for independent subsystems could be adopted unchanged for the description of the full system. An a posteriori confirmation of the chosen step-wise approach is given by the sensitivity analysis with respect to the adjustable parameters presented in appendix A.

5. Conclusions and outlook

A mechanistic model for the dehydrogenation of ethylbenzene to styrene over single crystal iron oxide films is derived and parameterised based on a combined surface science and chemical engineering approach. The experimental data used for parameter fitting originate from TDS measurements in ultra high vacuum and conversion measurements in a micro reactor. The conversion measurements comprise the transient behaviour of increasingly complex subsets of the considered reaction system. In addition, off-line surface analysis by LEED, AES and TPO provides insight into surface composition and coverage by carbon deposits.

A stepwise procedure has been applied for determining the parameters of the kinetic model following the order of the conversion experiments. An excellent agreement between modelling and experimental results is attained. The results confirm that the behaviour of the single crystalline surface can be described with a continuum model as a function of macroscopic variables (catalyst composition, gas phase composition, surface coverage). Hence, the model is compatible with commonly used reactor models in chemical engineering and can be regarded as the first step towards utilizing the knowledge gained from analyses of the ideal system under well-defined conditions in understanding and modelling technical catalysts. In a next step the focus will be set on modelling porous catalysts assessing whether they can be described adequately by superposition of the above kinetic model valid for the single crystal surface and an adequate pore model accounting for diffusional transport.

Acknowledgements

We acknowledge the financial support of the Deutsche Forschungsgemeinschaft, DFG (KO2049/2-2 and RA376/2-2). Our special thanks go to Prof. G. Eigenberger and Prof. G. Veser.

Appendix A

Sensitivity analysis provides a compact and simplified picture of the significance of the model parameters on the residual of the optimization problem. Sensitivity diagrams display the dependence of a characteristic on the significant parameters. The characteristic is usually a quantity of practical relevance derived from the state variables of the model, e.g. conversion, yield or selectivity. However, the selection of the characteristic and its normalization imposes certain arbitrariness on sensitivity analysis. In order to reduce arbitrariness to the minimum, the sensitivity analysis presented in the following uses the norm of the residual vector as characteristic. The residual vector of the optimization problem underlying the parameter fitting procedure includes information on ethylbenzene conversion, coke coverage and hematite fraction of the iron oxide surface. These quantities are used as characteristics in the following analysis. The sensitivity is generally defined as follows:

$$S_{i,j}(t) = \frac{\left(\Phi_i\left(k_j^{ref} + \Delta k_j, t\right) - \Phi_i\left(k_j^{ref}, t\right)\right) \cdot k_j^{ref}}{\Phi_i\left(k_j^{ref}, t\right) \cdot \Delta k_j}$$

$$\Phi_i = \left\{X_{EB}, N_{coke}, x_{Fe_2O_3}\right\}$$

represents the characteristic and k_j the adjustable parameter. The characteristic is obviously time dependent. Therefore, the mean value of the R^1-norm is computed over the measurement interval of an experimental run:

$$\overline{S}_{i,j} = \frac{1}{t_{end} - t_{begin}} \cdot \int_{t_{begin}}^{t_{end}} \left| S_{i,j}(t) \right| \cdot dt$$

Figure A1 displays the sensitivity diagrams corresponding to the three experimental series used for parameter fitting (corresponding to Figures 3, 4, 5). The sensitivities of the three characteristics are included in each diagram. The parameters adjusted to the respective experimental run are indicated by star. Clearly, the model is sensitive with respect to the parameters assigned to each subsystem.

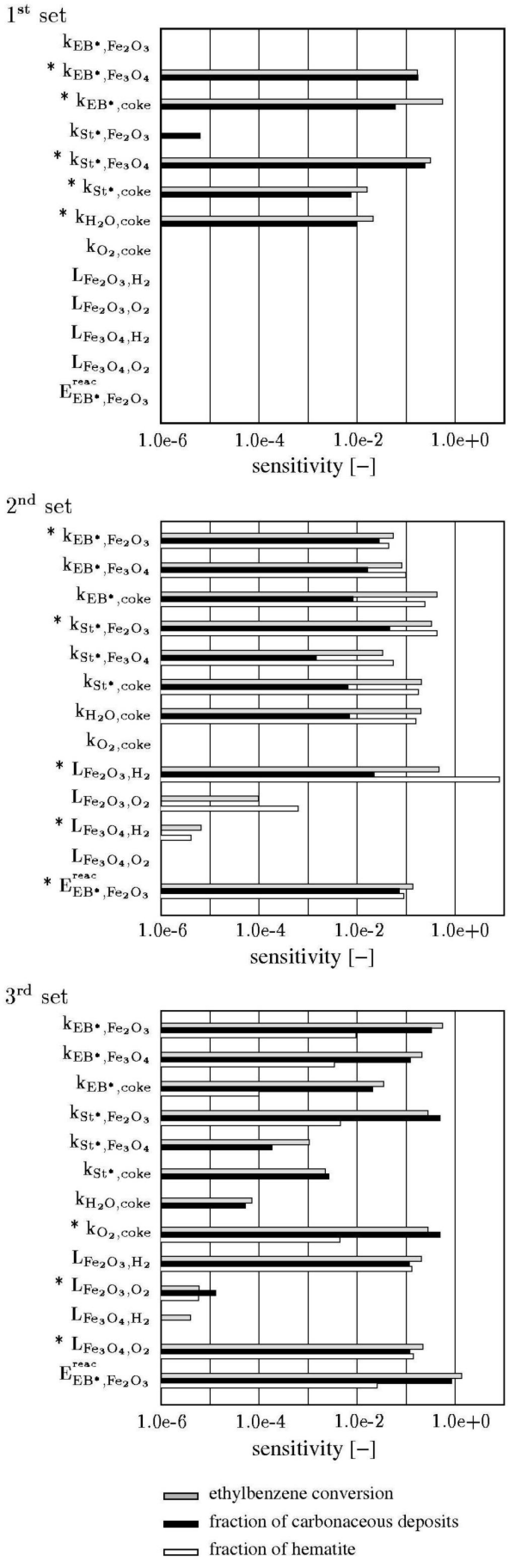

Figure A1:
Sensitivity diagrams corresponding to the three steps of parameter fitting procedure.

Nomenclature

N	number of moles of a component [mol]
N_{Fe}	number of moles of iron in the catalyst sample; $6{,}55*10^{-8}$ [mol]
J	component mass exchange terms [mol/s]
F	flow [mol/s]
$n_s^{sat.}$	molar surface specific concentration of adsorbed species; $332{,}23*10^{-12}$ [mol/cm^2]
a_{coke}	molar surface area of carbonaceous deposits; $1{,}143*10^{9}$ [cm^2/mol]
A_0	total surface area; 0,50 [cm^2]
A	surface area [cm^2]
p	partial pressure of gas phase component [Pa]
T	temperature [K]
R	general gas constant [J/mol.K]
M	molar mass of gas phase component [g/mol]
σ	sticking coefficient of gas phase component in adsorption relation; all equal to 1.0 [-]
Θ	surface coverage [-]
E	activation energy [J/mol]
f	frequency factor of surface species in desorption relation [1/s]
k^0	frequency factor of surface reaction [1/s]
T_0	treshold temperature in surface reaction relation; 773,0 [K]
L	frequency factors in phase transformation relation [mol^2.K/J.s]
ν	stochiometric coefficient of redox reactions of the iron oxides [-]
μ	chemical potential of component in phase transformation relation [J/mol]
x	molar fraction of iron oxide [mol/mol]

Subscript indices

j	gas phase component
k	adsorbed specie
s	surface specie
i	surface reaction
l	specie participating in redox reaction
p	iron oxide reactant of redox reaction
q	gas phase reactant of redox reaction

Superscript indices

0	inlet
gas	gas phase
ads	adsorption
des	desorption
reac	reaction

References

[1] Dumesic, Rudd, Aparicio, Rekoske, Trevino, *The Microkinetics of Heterogeneous Catalysis*, American Chemical Society, Washington, DC, 1993.
[2] G. Ertl, Journal of Vacuum Science & Technology A **1** (1983) 1247.
[3] P. Stoltze, J. K. Norskov, Physical Review Letters **55** (1985) 2502.
[4] M. Bowker, I. B. Parker, K. C. Waugh, Applied Catalysis **14** (1985) 101.
[5] R. Schlögl, in: G. Ertl, J. Knözinger, J. Weitkamp (Eds.), Handbook of Heterogeneous Catalysis, VCH, Weinheim, 1997, Vol. 4, Chap. 2.1.
[6] G.R. Meima, P.G. Menon, Appl. Catal. A **212** (2001) 239.
[7] O. Shekhah, W. Ranke, A. Schüle, G. Kolios, R. Schlögl, Angew. Chem. Int. Ed. **42** (2003) 5760.
[8] N.N. Lebedev, G.V. Odabashyan, V.V. Lebedev, M.G. Makorov, Kinet. Katal. **18** (1978) 1177.
[9] S.S.E.H. Elnashaie, B.K. Abdalla, R. Hughes, Ind. Eng. Chem. Res. **32** (1993) 2537.
[10] G. Kolios, G. Eigenberger, Chem. Eng. Sci. **54** (1999) 2637.
[11] J.D. Snyder, B. Subramaniam, Chem. Eng. Sci. **49** (1994) 5585.
[12] A.A. Savoretti, D.O. Borio, V. Bucala, J.A. Porras, Chem. Eng. Sci. **54** (1999) 205.
[13] M. Muhler, R. Schlögl, G. Ertl, J. Catal. **138** (1992) 413.
[14] S. K. Shaikhutdinov, Y. Joseph, C. Kuhrs, W. Ranke, W. Weiss, Faraday Discussions **114** (1999) 363.
[15] Y. Joseph, W. Ranke, W. Weiss, Journal of Physical Chemistry B **104** (2000) 3224.
[16] C. Kuhrs, Y. Arita, W. Weiss, W. Ranke, R. Schlögl, Topics in Catalysis **14** (2001) 111.
[17] W. Ranke, Y. Joseph, Phys. Chem. Chem. Phys. **4** (2002) 2483.
[18] W. Weiss, W. Ranke, Progress in Surface Science **70** (2002) 1.
[19] O. Shekhah, W. Ranke, R. Schlögl, J. Catal. **225** (2004) 56.
[20] W. Ranke, O. Shekhah, Recent Res. Dev. Surface Sci. **1** (2004) 75.
[21] C. Kuhrs, M. Swoboda, W. Weiss, Topics in Catalysis **15** (2001) 13.
[22] M. Guisnet, P. Magnoux, Appl. Catal. A **212** (2001) 83.
[23] F.D. Kopinke, G. Zimmermann, G.C. Reyniers, G.F. Froment, Ind. Eng. Chem. Res. **32** (1993) 2620.
[24] B. Amami, M. Addou, C. Monty, Defect and Diffusion Forum **194-199** (2001) 1051.
[25] Krylov, Shub, *Nonequilibrium processes in catalysis* , CRC Press, London, 1994, p. 187.
[26] R. Zacharia, *Desorption of gases from graphitic and porous carbon surfaces*, Dissertation, FU Berlin 2004.